ISSN 2007-9737

Deep Learning–Driven Automated Grading of Astrocytoma from Brain MRI Using an Enhanced DenseNet-169 Framework

Muhammad Afzaal Akhtar[1], Ghulam Gilanie[1], Muhammad Sajid[1,2], Maryam Mazher[2], Muhammad Abbas[1], Oswaldo Morales Matamoros[2,*]

[1] The Islamia University of Bahawalpur,
Faculty of Computing, Department of Artificial Intelligence, Bahawalpur, Pakistan

[2] Instituto Politécnico Nacional,
Centro de Investigación en Computación, Mexico City, Mexico

{msajida26, mmazhera26, omoralesm}@cic.ipn.mx, ghulam.gilanie@iub.edu.pk,
{afzaalakhtar07, abbasbwn1076}@gmail.com

Abstract. Astrocytoma represents one of the most widespread categories of primary brain tumors, with higher-grade variants linked to aggressive progression and poor survival outcomes. Conventional diagnostic techniques, including biopsy procedures, are invasive and may introduce clinical risks. This study aims to develop an artificial intelligence-based, non-invasive framework for automated grading of astrocytoma using brain magnetic resonance imaging (MRI). Methods: A dataset of brain MRI images compiled retrospectively was collected from the Radiology Department of Bahawal Victoria Hospital, Bahawalpur, Pakistan. Multiple pre-trained convolutional neural network architectures namely ResNet-152, VGG-19, and MobileNetV3 were implemented using transfer learning for comparative evaluation. An optimized DenseNet-169 model was proposed, incorporating fine-tuning strategies, advanced regularization, and attention-inspired feature learning to improve classification performance. Standard preprocessing and data augmentation techniques were applied. The model's performance was evaluated by accuracy, precision, recall, F1-score, and AUC-ROC metrics under a consistent validation protocol. Results: The proposed DenseNet-169-based framework demonstrated superior classification capability, achieving an accuracy of 99.68%, and outperformed ResNet-152 (96.34%), VGG-19 (95.22%), and MobileNetV3 (97.42%). The model also exhibited strong generalization performance across evaluation metrics. Conclusions: The presented approach offers an effective and non-invasive solution for astrocytoma grading using MRI data. Integrating deep learning techniques improves diagnosis accuracy and may aid clinical decision-making, especially in resource-limited healthcare environments. The proposed framework emphasizes the potential of artificial intelligence to advance medical image analysis and improve patient outcomes.

Keywords: Astrocytoma classification, brain MRI analysis, deep learning in medical imaging, transfer learning, DenseNet-169, tumor grading, artificial intelligence in healthcare, radiological image classification, CNN-based diagnosis.

1 Introduction

Development of deep learning has also led to an increase in the need for smart gadgets' in-built processing capacity [1]. Medical characteristics are one of the more challenging parts of diagnosis, and their early identification could save potentially fatal circumstances [2]. This generally necessitates the creation of a more straightforward, accurate, and safe diagnostic technique. Nowadays, most techniques for detecting brain cancers are invasive [3].

Tissues and organs, which are mixture of microscopic units which are called cells, make up the human body [4]. The human body grows, heals, and repairs itself through the controlled division of cells to create new cells. For instance, a cell gets a signal telling it to die if it is unable to repair itself [5]. A cancer is formed when cells'

consistent activity is disrupted and they start to split that is wildly [6]. When the cells' normal function is disturbed and they start to divide uncontrolled, a tumor is formed [7].

The abnormal growth of cells that invade or spread to other parts of the body is called cancer. When suspicious symbols are observed, a medical expert may advise the excision of a small sample of dis-eased tissue. Clinically, this entire process which involves both cell removal and decision-making is called a biopsy [8]. Biopsy procedures determine the presence of an anomaly as well as its extent [9]. This is riskier and requires more time to heal. Coma, seizures, stroke, infections, brain hemorrhage, or edema are some of the possible outcomes [10].

If there are no cancerous tissues present, the infected cells are benign; if they do, they are malignant. Benign tumors grow slowly and don't usually propagate to other sections of the body [11]. They turn into harmful when they are defined strain on adjacent organs [12]. They become troublesome when they place strain on organs that are adjacent [13]. Malignant tumors differ significantly from normal tissues in terms of their cellular structure [14]. Their quick growth makes them invasive rather than benign [15].

Tumors are diagnosed during surgical procedures based on the proliferation rate (mitotic activity) and the existence of cells (nuclear atypia) [16]. Dysfunction in the nucleus and cell division will serve as crucial indicators, in addition to characteristics, for assisted by machines automatic classification, then the application of cellular or genetic data to grade images of cancerous tissues will effectively represent [2].

Cancer can start in the cerebral cortex itself (the main tumor) or via metastasis from some other place to the central nervous system (metastasized tumor), just like it can in other organs [17]. Brain cancers hardly ever spread to other bodily organs [18]. Benign tumors may be categorized as if discovered in regions that regulate vital processes like respiration, malignant because they have the potential to be lethal [19]. When treating secondary tumors, the initial site is usually considered. Knowing the initial site of the tumor helps with the selection of secondary cancer treatment. More than 120 types of brain tumors exist [20]. The WHO's categorization system is employed to categorize different types of brain tumors. All brain tumors are classified according to their genesis and cell activity. A higher grade indicates that the tumor is more aggressive or poses a greater threat. Grade I to Grade IV tumors are classified according to how quickly they grow. The stage of the tumor may also be used to describe it. It is used to find out whether a tumor has spread. To help medical professionals, tumor staging, grading, and classification are used. Practitioners can more effectively discuss a tumor, offer treatment suggestions, and learn more about the patient's status and diagnosis by employing this terminology [21].

The human brain contains approximately 86 billion neurons, with grey matter mainly composed of neuronal cell bodies, dendrites, and synapses, while white matter primarily consists of myelinated axons. Immune cells, particularly microglia, surround and support nerve cells by protecting them and maintaining neural function [22]. Another way to classify them is astrocytes, oligodendrocytes, such as cells of the endothelial system. Star-like glial cells are called astrocytes. They might be additionally categorized as astrocytes, oligodendrocytes, ependymal precursor cells, etc.

Grade-II astrocytes, illustrated in Fig. 2, exhibit moderate growth yet possess the ability to disseminate to adjacent areas tissues. While typically benign, it may progress too malignant [25]. Gradual proliferation, sporadic encroachment of additional brain areas, unclear boundaries, incidence in individuals aged 20 to 50, and frequency among younger individuals with seizures were the characteristics among individuals with low-grade astrocytoma that were either under- or well-treated.

As illustrated in Fig. 3, Grade III astrocytes are neoplastic malignancies that belong to the anaplastic class. It is more aggressive than Grade-II astrocytoma, usually invades surrounding tissue, has irregularly shaped tumuli, affects Individuals of both genders aged 30 to 50, with a higher prevalence in males than females.

As illustrated in Fig. 3, Grade III astrocytes are neoplastic malignancies that belong to the anaplastic class. It is more aggressive than Grade-II astrocytoma, usually invades

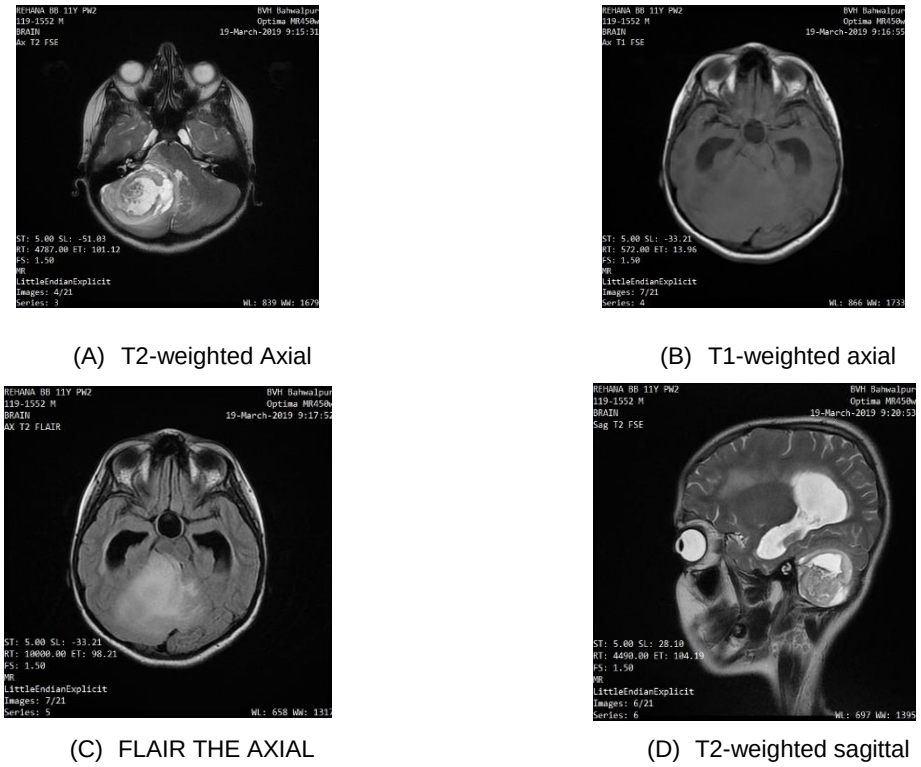

(A) T2-weighted Axial

(B) T1-weighted axial

(C) FLAIR THE AXIAL

(D) T2-weighted sagittal

Fig. 1. Illustration characteristics of Grade I Astrocytoma (Pilocytic Astrocytoma)

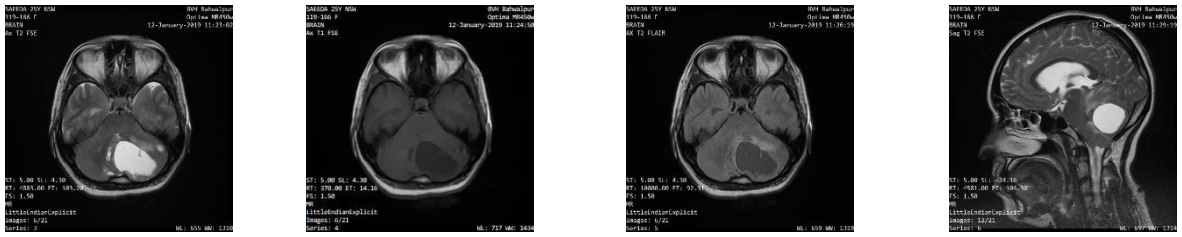

(A) T2-Weighted AXIAL

(B) T1-Weighted AXIAL

(C) FLAIR AXIAL

(D) T2W SAGITTAL

Fig. 2. Illustration characteristics of grade II astrocytoma

surrounding tissue, has irregularly shaped tumuli, affects individuals of both genders aged 30 to 50, with a higher prevalence in males than females.

A cancerous neoplasm that predominantly grows in the bisection of the brain but may also originate in the cervical spine or the brainstem, Glioblastoma Multiforme (GBM), commonly referred to as grade-IV astrocytoma, is depicted in Fig. 4.

It is almost tough to eradicate since it continuously infiltrates and invades surrounding tissue [26]. In addition to several other medical imaging techniques, astrocytoma diagnosis, monitoring, and characterization depend heavily

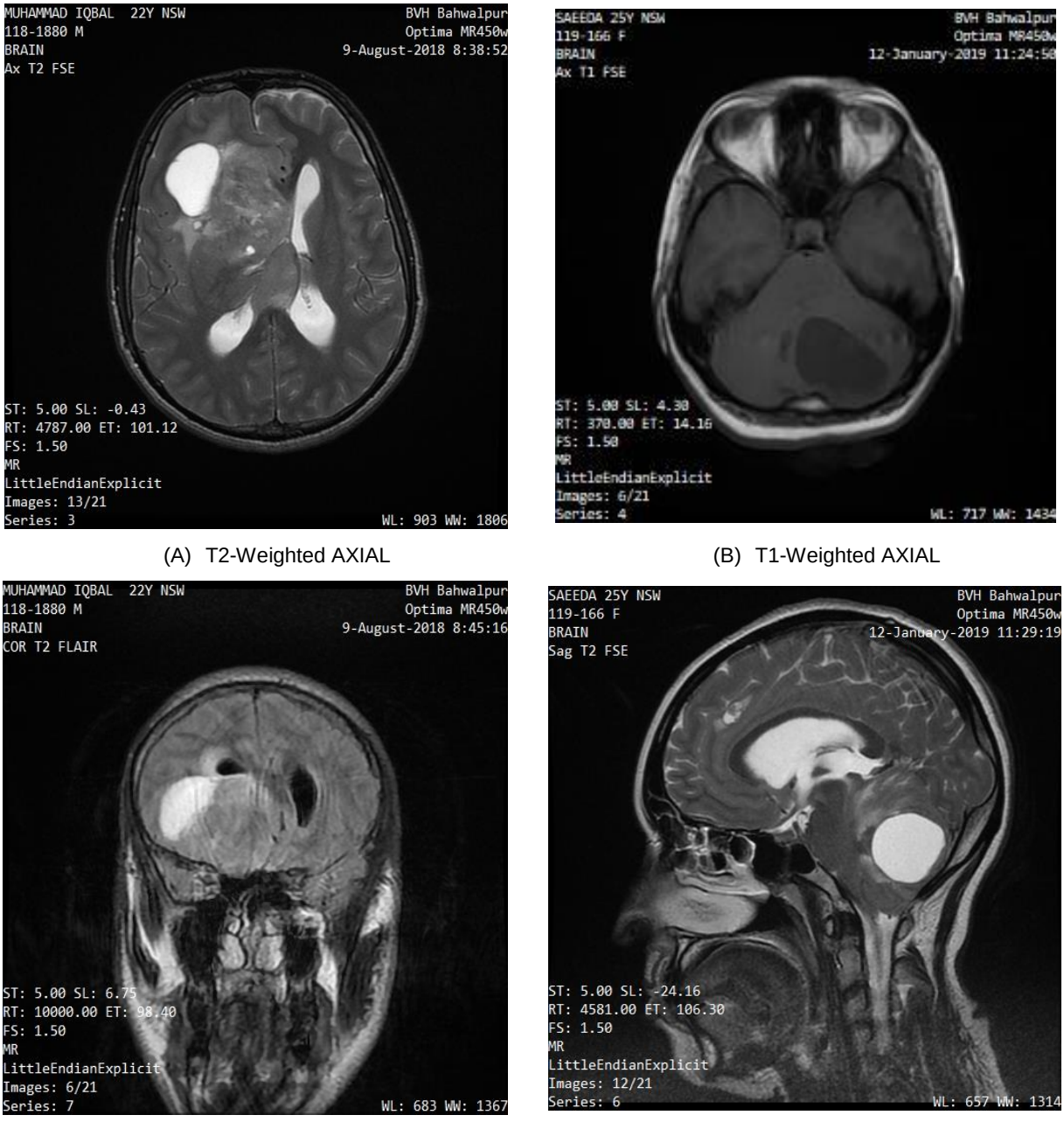

(A) T2-Weighted AXIAL

(B) T1-Weighted AXIAL

(C) FLAIR SAGITTAL

(D) T2W SAGITTAL

Fig. 3. Illustration characteristics of grade III Astrocytoma (Anaplastic Astrocytoma)

on Magnetic Resonance Imaging (MRI), which uses T1-weighted (T1w), T2-weighted (T2w), and Fluid-Attenuated Inversion Recovery (FLAIR) imaging sequences. Comprehensive tissue analysis is provided by these high-resolution MRI techniques. Most often found in men, GBMs are made up of many cell types and can either form directly or expand from a low-grade astrocytoma.

Recent tomography has enhanced the capacity to extricate between malignant and regular cells.

The major objective is to detect astrocytoma in brain MRI scans and includes the following:

- To suggest a strategy for combining transformer learning-based designs with multi-modal MRI data to increase accuracy and reliability of astrocytoma grading while taking different imaging sequences and patient demographics into account.
- To enhance the quality and consistency of MRI images and optimize pre-trained architecture, guaranteeing efficient learning and generalization from a variety of datasets.
- To evaluate the efficacy of the suggested astrocytoma grading system with current grading techniques and assess its performance through comprehensive validation using industry-standard metrics and actual clinical data.

The present work's significant contributions are presented below.

- The study suggests a better way to use several MRI sequences, including FLAIR, T1w, and T2w, to increase the astrocytoma grading system's accuracy and comprehensiveness.
- To prove its superior performance using clinical datasets and accepted evaluation measures, the suggested strategy is anticipated to undergo an accurate validation process in contrast to current grading systems.
- The study provides examples of the model's application in clinical settings, demonstrating how it might enhance diagnostic precision and assist in patient treatment planning.

2 Literature Review

This paper [27] offers an automated deep learning model and the finest information fusion framework for classifying brain tumors based on MRI images. The performance of the model was impacted by the severe nature of the data set employed. To solve this problem, a sparse autoencoder network was created. Two pre-trained neural networks were subjected to deep feature extraction using an improved Quantum Theory-based Marine Predator Optimization algorithm (QTbMPA). The framework improved accuracy to 99.80%, precision to 99.83%, sensitivity to 99.83%, and false negative rate to 17%.

The study [28] evaluated the diagnostic performance of the self-attention-based Variable Vision Transformer (vViT) model in predicting the grade of diffuse gliomas using the WHO's 2021 classification of central nervous system (CNS) malignancies. Gliomas were predicted by the model using radiometric features, age, sex, and four MRI sequences. For the multiclass classification (classes 2 vs. 3 vs. 4) and the binary classification (class 4 vs. classes 2/3), the greatest accuracy and AUC-ROC were found to be 0.84 (95% CI: 0.75–0.93) and 0.94 (95% CI: 0.88–0.98), respectively. Furthermore, the multiclass classification had the greatest Cohen's κ coefficient, demonstrating a high degree of agreement between the ground truth and predicted labels.

This article [29] introduces BrainCDNet, a unique Deep Learning (DL) architecture that uses batch norm and global average pooling to establish weights and concatenates pooling layers to address overfitting issues. The model identifies images using binary and multiclass MRI database features. According to empirical data, the reported model outperformed state-of-the-art techniques with noteworthy accuracy on both datasets: 96.78% (multiclass) and 99.45% (binary).

This study [30] used the BraTS2018 dataset to segregate the substructure of brain tumors, including necrosis and non-enhancing, edema, and enhancing areas. The proposed grading model is then trained on these locations. Additionally, they used 69 samples from a dataset from a tertiary hospital to examine the effectiveness of their model. Accuracy values of 0.85 and 0.87 were obtained using the BraTS2018 test sample and the tertiary hospital dataset, respectively. This consistent score on both public and tertiary hospital datasets indicates the model's reliable and steady performance.

Table 1. Summary of the existing literature review

Reference	Methodology	Dataset Used	Evaluation Measures	Problem Addressed
[27]	sparse autoencoder and QTbMPA	Figshare brain tumor dataset	Accuracy: 99.80%, Sensitivity: 99.83%, Precision: 99.83%, False Negative Rate: 17%	A few irrelevant features were selected for the classification
[28]	vViT	2021 WHO CNS tumor classification dataset	AUC-ROC were 0.84, multiclass classification (2 vs. 3 vs. 4), and 0.94 (0.88–0.98)	Predicting the grade of diffuse gliomas
[29]	BrainCDNet (deep learning architecture)	Two Brain MRI datasets: Binary (healthy vs. pathological) and multiclass (glioma vs. pituitary)	Accuracy: 99.45% (binary), Accuracy: 96.78% (multiclass)	Ignoring the noise and unpredictability of real-world medical imaging circumstances
[30]	Tumor substructure segmentation and grading model	BraTS2018 and the tertiary hospital dataset	Accuracy: 0.85 (tertiary hospital), Accuracy: 0.87 (BraTS2018)	Limited generalization and high computation
[31]	Transfer to learning-based measurement strategy using optimized Efficient Nets	meningioma, glioma, and pituitary tumor classifications	Accuracy: 98.48%, Recall: 98%, Precision: 98.5%, Sensitivity: 98.71%	Brain tumor classification using various datasets
[32]	OSVMK	Brain tumor MRI images	Accuracy: 95.20%, Precision: 97.87%, Recall: 96.48%, Specificity: 96.45%	Tumor grading and segmentation
[33]	3D FL scheme for glioma classification	TCGA, US, and MICCAI datasets	Test accuracy: 85.46% (IDH subtypes), 75.56% (Glioma grades), 89.28%, and 90.72% (Glioma grades)	Brain tumor classification using various datasets

This study [31] presents a transfer learning-based measuring approach for classifying brain growths into distinct categories across three distinct datasets, including pituitary growth, glioma, and meningioma.

The three distinct classification findings that were produced because of using an efficient net-based transfer learning mechanism are presented in this paper. Based on the use of EfficientNetV2S as the system, this method of fine-tuning the pre-trained EfficientNetV2S outperformed the current methods on all datasets. The effectiveness of the proposed model has been evaluated using performance measures, and the outcomes obtained have been contrasted with those of cutting-edge techniques. The average accuracy, recall, precision, and sensitivity test scores are 98.48%, 98%, 98.5%, and 98.71%, respectively.

This paper [32] presents an online method that combines a new and effective tumor segmentation technology with an inventive optimization strategy for completely automated brain tumor grading in MRI data. The two main characteristics used for tumor segmentation are edge information and tumor appearance intensity. Characteristics of the impacted area are then retrieved. A Support Vector Machine with Kernel (OSVMK) augmented by dynamic fuzzy rule-based parameter optimization is then used to grade the tumor.

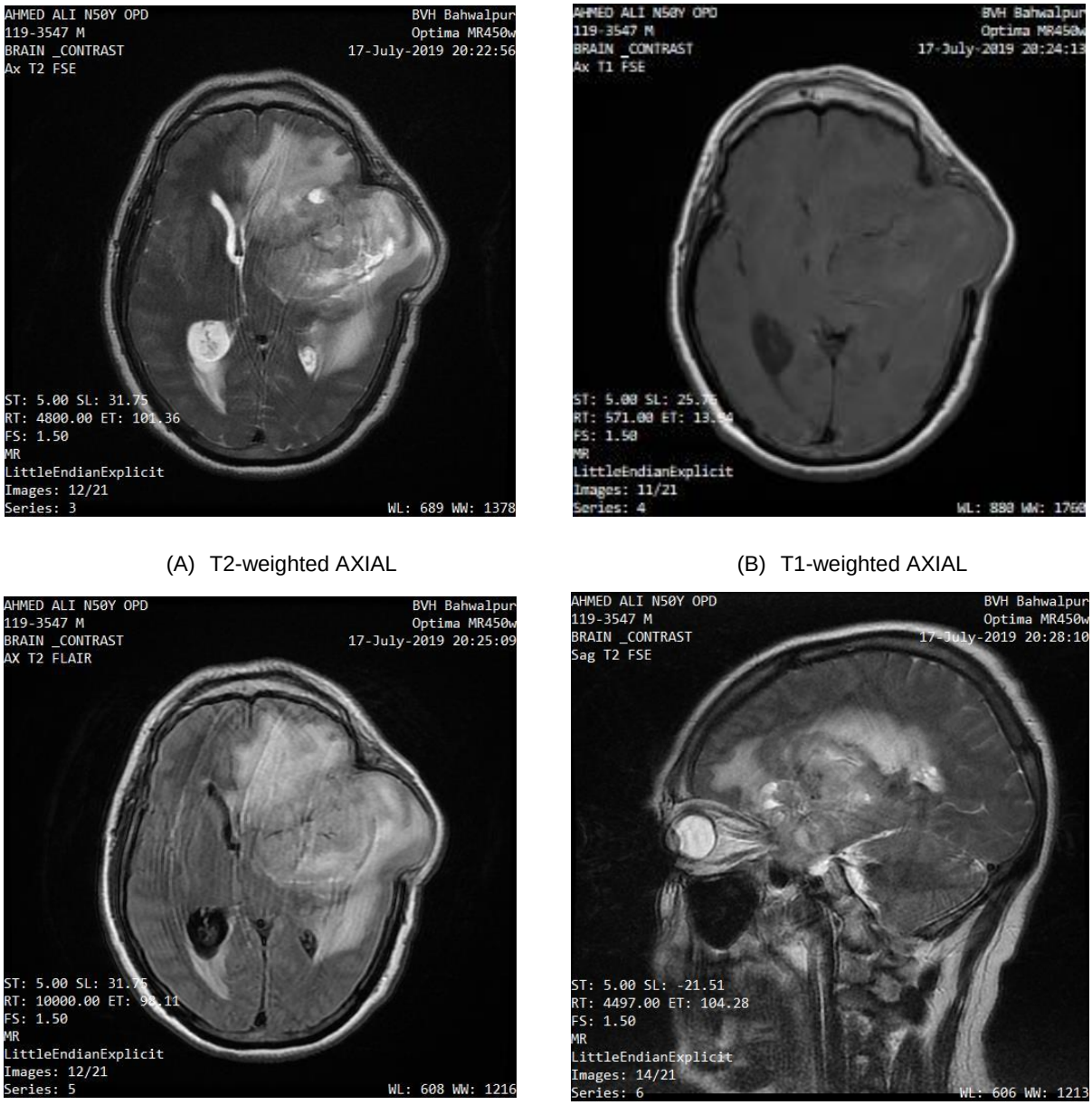

(A) T2-weighted AXIAL

(B) T1-weighted AXIAL

(C) FLAIR THE AXIAL

(D) T2-weighted sagittal

Fig. 4. Illustration characteristics of grade III Astrocytoma (Anaplastic Astrocytoma)

Manual segmentation using similarity criteria was used for comparison to assess the suggested segmentation approach. The accuracy, precision, recall, specificity, and execution time of the tumor grading performance were evaluated and compared between the batch SVM with kernel (batch SVMK), the suggested online technique, and a traditional online approach.

High agreement between the segmentation results and expert manual annotations was

observed. Furthermore, with accuracy, precision, recall, and specificity scores of 95.20%, 97.87%, 96.48%, and 96.45%, respectively, the suggested approach showed excellent grading performance.

The study [33] offers a slice-based deep learning classifier, domain mapping, an improved federated dynamic method, and 3D scan-based post-processing to present a 3D federated learning (FL) framework for glioma classification. The objective is to compare performance across different FL algorithms to replace centralized learning (CL). The MICCAI dataset for glioma grade classification (high-grade vs. low-grade gliomas) and the TCGA and US datasets for glioma subtype classification (Isocitrate Dehydrogenase mutant vs. wild type) were used in the experiments. The FL method only slightly decreased accuracy when compared to CL (-1.17%, -0.83%), achieving test accuracy of 85.46% and 75.56% for IDH classification and 89.28% and 90.72% for grade classification. These findings demonstrate FL's feasibility as a substitute for centralized approaches.

2.1 Research Gap Established

There is yet no solution for the non-invasive grading of astrocytoma's using MRI scans without the need for surgery or biopsy. Overfitting and inadequate generalization are problems with current models, particularly when handling complicated, high-dimensional data. Transformer learning-based models are underutilized in astrocytoma grading and medical imaging, despite their superiority in identifying long-range relationships in data. Although there is little study on how to harmonize these techniques, integrating CNNs with transformer learners may provide a more comprehensive solution. The unbalanced character of medical datasets, which is essential for clinical decision-making, is another issue that the existing models have.

3 Materials and Methods

A thorough explanation of the dataset, methods, and processes used in the proposed approach is provided in this section.

3.1 Dataset

The Radiology Department (Diagnostics) at Bahawal Victoria Hospital, Bahawalpur, Pakistan, provided the MRI dataset. It contains 343 people's MRI scans, which were used to train, test, and validate the suggested model. 56% of the patients are male and 44% are female, and their ages range from 28 to 67.

Classified into astrocytoma grades, this dataset includes 80 individuals contributing 9,600 slices in Grade I, 91 individuals contributing 10,920 slices in Grade II, 87 individuals contributing 10,440 slices in Grade III, and 85 individuals contributing 10,200 slices in Grade IV. Three MRI sequences—T1w, T2w, and Flu-id-Attenuated Inversion Recovery (FLAIR) are included in each subject's dataset. To increase the model's flexibility and enable it to handle scenarios where only one sequence or direction is available, T1W and FLAIR were acquired in the axial plane, whereas T2W images were acquired in both the axial and sagittal planes. Three-dimensional anatomical sequences (TR=2s, TE=30ms, FOV=20cm, 512x512 resolution) were used for the scans, which were performed on a Philips Medical Systems system. Each sequence produced 30 slices possessing a thickness of 5mm without an interslice hole. Each subject, therefore, contributes 120 slices (30 for T1-weighted Axial, FLAIR Axial, T2-weighted Axial, and T2-weighted Sagittal). To further augment the dataset, every segment was rotated by 7 angles, resulting in a large, diverse dataset including 288,120 entries across Grades I-IV. This rotational augmentation was key to effectively training and evaluating the model for classifying astrocytoma grades.

3.2 Preprocessing

The N4ITK approach is utilized for rectifying the distortion of the bias field, experienced in MRI images, ensuring that the effective tissues of the same type are uniform across the several images. To accommodate comparable intensity levels and contrasts among individuals and transactions, intensity normalization is applied to each sequence. The purpose of this work is to grade astrocytoma tumors in ground truth and k-means

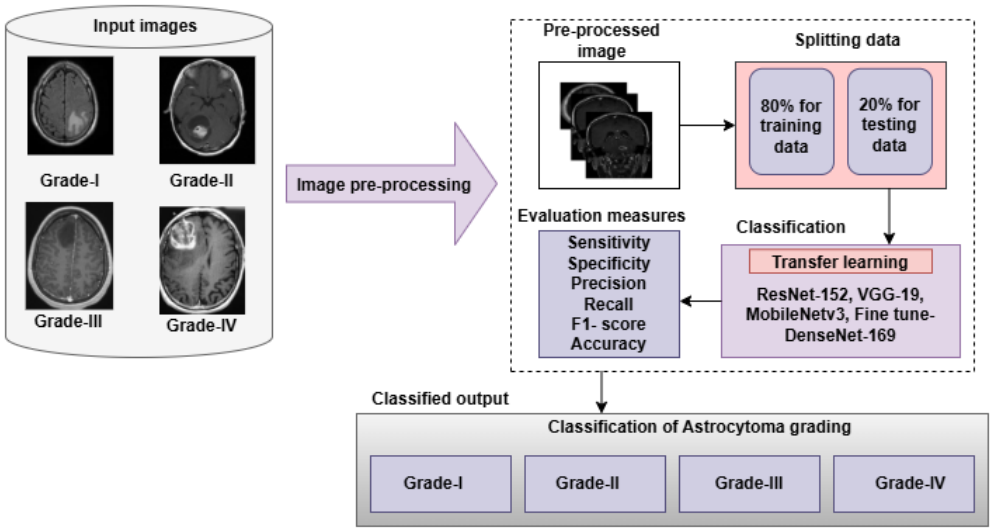

Fig. 5. Overall proposed methodology

clustering pictures. There are several sets of tasks involved in the preprocessing stage, including normalization, noise reduction, skull stripping, resampling, and augmentation. Noise reduction eliminates unwanted features, normalization flattens intensity levels, and skull stripping re-moves the brain area for improved analysis. To make the dataset more stable, augmentation techniques enlarge it beyond its actual size, while resampling ensures that the dataset is consistent. To distinguish between astrocytoma grades, previously processed images are divided into segments. For 80 patients with Grade-I astrocytoma's, there are 9,600 slices accessible, each including 120 slices of various sequences. The four slices containing the largest tumor area are rotated using three different angles to address the random growth of tumors, yielding 28,800 slices for Grade I. 10,920 slices are provided for 91 patients with Grade-II astrocytoma. 32,760 slices are used for the studies; after 4 slices with the greatest tumor portion are designated, they are alternated in these directions. Using rotational techniques for each grade, the same procedure is used for Grade III and Grade IV astrocytoma. Eq (1) is implemented to normalize the input image to the constrained range of 0 to 1. "Z" denotes the input brain MRI of dimensions (mxn), while the normalized MRI is designated as "Dnorm":

$$Z_{norm=\frac{Z-\mu}{\sigma}}. \tag{1}$$

Eq. (2) explains how to use a filter such as Gaussian smoothing to smooth out MRI pictures in order to eliminate noise and undesired artifacts:

$$I_{filtered}(a,b) = \frac{1}{x}\sum_{i=-k}^{k}\sum_{j=-k}^{k} I\,(a+i, b+j)\,, \tag{2}$$

where I (a, b) denote the original image, G (i, j) represents the Gaussian kernel.

The method employed to extract non-brain tissues from MRI images in order to isolate the brain region for comprehensive investigation is delineated in Eq. (3):

$$I_{b=}I - I_s\,. \tag{3}$$

Eq. (4) delineates the methodology for standardizing the voxel dimensions and spatial resolution of MRI images to a consistent scale across all samples:

$$I_{resampled}(a,b) = I\big(f(a), f(b)\big)\,. \tag{4}$$

Based on Eq. 5, the original images were augmented using a rotation-based enhancement technique, in which each image was rotated by 45°, 90°, 135°, 180°, 225°, 270°, and 315° to increase the number of training samples:

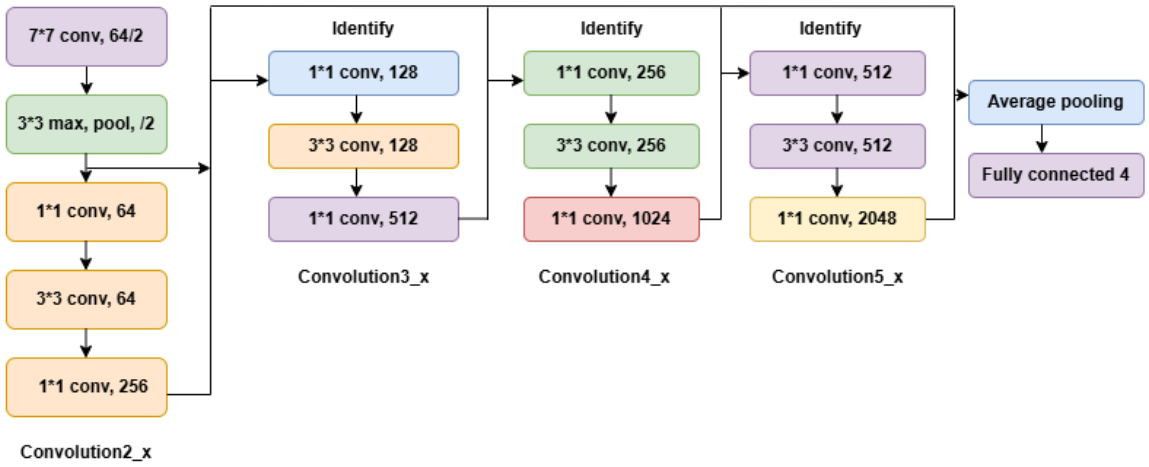

Fig. 6. Architecture of ResNet-152

$$I_{rotated}(a', b') = I\ (a\ cos\theta - b\ sin\theta + b\ cos\theta)\ . \quad (5)$$

3.3 Models for Transfer Learning

The total process, as illustrated in Fig. 5, creates four classes for assessing and predicting this structure using an improved DenseNet-169 and three well-known transfer learning techniques: Res-Net-152, VGG19, and MobileNetv3. These architectures were selected for their demonstrated capacity to address image categorization problems, especially in medical imaging. DenseNet-169 was selected for its dense connections which improves feature propagation and reuse; MobileNetV3 was picked for its lightweight architecture, suitable for real-time applications; ResNet-152 for its deep residual learning capabilities; and VGG-19 for its depth and simplicity. These methods are applied to the data, which is then divided into a training set (80%) and a test set (20%) following the analysis.

Transfer learning, particularly in NLP and image recognition, permits a model to be trained on a single task to be effectively adapted to a related task, saving time and effort. As an alternative to developing a model from scratch, this approach also entails modifying an existing model trained on a sizable dataset, in this case, the grading of astrocytoma's. The transformer learner is adjusted to account for the many characteristics of brain MRI images. Additionally, this makes it easier for the student to classify various astrocytoma grades. Astrocytoma's of various grades can be graded more accurately and effectively with transfer learning, reducing the time and resources required for training. To ensure that every model was comparable, the input RGB image size of 224x224 was used for each transfer learning. A common feature of many deep learning applications, including object identification, picture classification, and even illness detection, is transfer learning.

3.3.1 ResNet-152

The initial layer of ResNet-152 is a convolutional layer that utilizes 64 filters of size 7x7 on the MRI image. This is essential because it makes it easier for the network to learn broader information, such as the tissue structures in an MRI image of the brain, by reducing spatial dimensionality. To assist in directing the network's attention to highly noticeable areas, such as the outline of a potential tumor or other ab-normality, the 3×3 max pool layer's dimension is then further reduced. There are three convolutional layers in the very next block. The first one decreases the number of input channels while maintaining the same spatial dimensions and features 64 1x1 filters. Next, medium-level characteristics, such as tumor boundaries and textures, are captured using a convolutional layer with 64 3x3 filters. As the final process prior to the data being utilized for further complex layer feature designs, the last 1x1 convolution increases the channels to 256. By

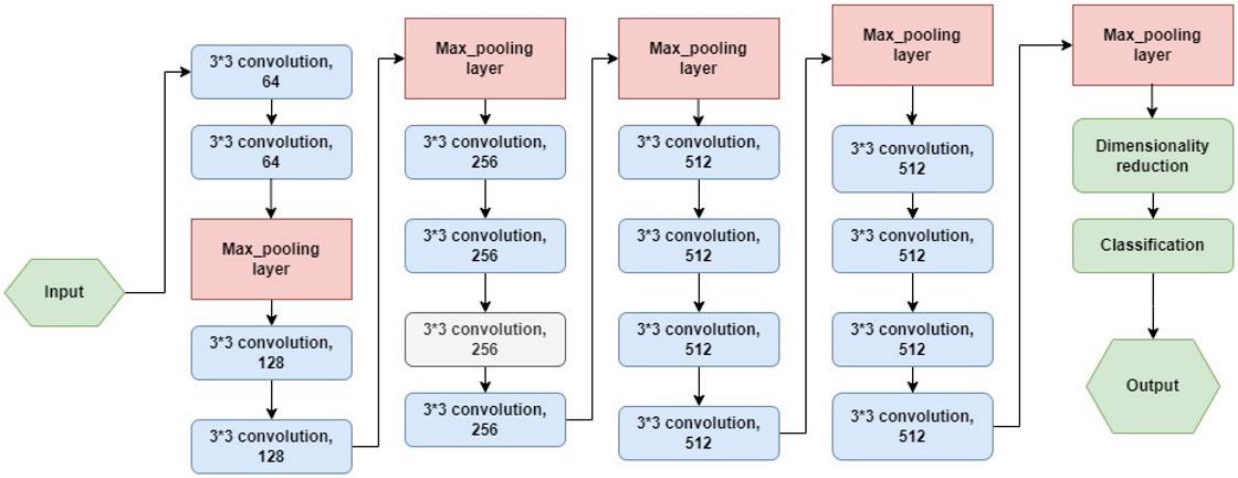

Fig. 7. VGG-19 architecture

employing 3x3 filters and increasing its depth to 128 channels, the network builds on the prior one, allowing it to learn a broader range of characteristics, as shown in Fig. 6. This layer examines more specific MRI image features to help differentiate between tumor grades. To accomplish the final classification, the final convolutional layer consists of 512 filters, with 1×1 and 3×3 convolutional layers, totaling 2048 channels, and captures abstract and detailed characteristics. The final classification is obtained by combining the features using average pooling and fully connected layer 4.

3.3.2 Visual Geometry Group 19 (VGG-19)

An expansion of the VGG16 architecture, the VGG19 architecture is among the top deep convolutional neural network (CNN) models. It Its 19 layers, consisting of 16 convolutional layers and 3 fully connected layers. Fine-scale textures and features in images can be captured by VGG19's deep architecture, which uses 3x3 convolutional kernels for feature extraction. Four convolutional layers are used by the VGG19 network to extract various attributes from MRI brain images as input. The small details are recorded in the first block's two convolutional layers, each of which has 64 filters. To capture intricate structures like patterns and contours, the second block uses 128 filters.

Four convolutional layers, each with 256 filters to capture high-level information, are what define the third block. To differentiate between astrocytoma grades, the filters are expanded to 512 in the fourth block. The last block, which addresses more complex characteristics that will be used at the end of the classification process, uses 512 filters in each layer once more. By reducing the size of the input space, max-pooling layers simplify the computations. Because the final layers are dense, it is easier to use the high-level information that the Convolutional layers have learnt to improve the assessments, as shown in Fig. 7. VGG19 uses the ReLU activation function to address nonlinearity.

3.3.3 MobileNetV3

The MobileNetV3 framework utilizes a preprocessed MRI scan with three color channels as input. Initially, low-level features such as gradients and edges are extracted using a 3x3 convolutional layer. Batch normalization uses the hard swish (h-swish) activation function to stabilize and accelerate training. The design comprises multiple bottleneck layers, with 1x1 convolutions, depth-wise convolutions, pooling operations, and fully linked layers. Fully connected layers and average pooling are used to extract geographical data, minimizing dimensionality and organizing the data for the ultimate classification phase. The final layer produces a 1280-dimensional feature vector that provides important information for tumor grading.

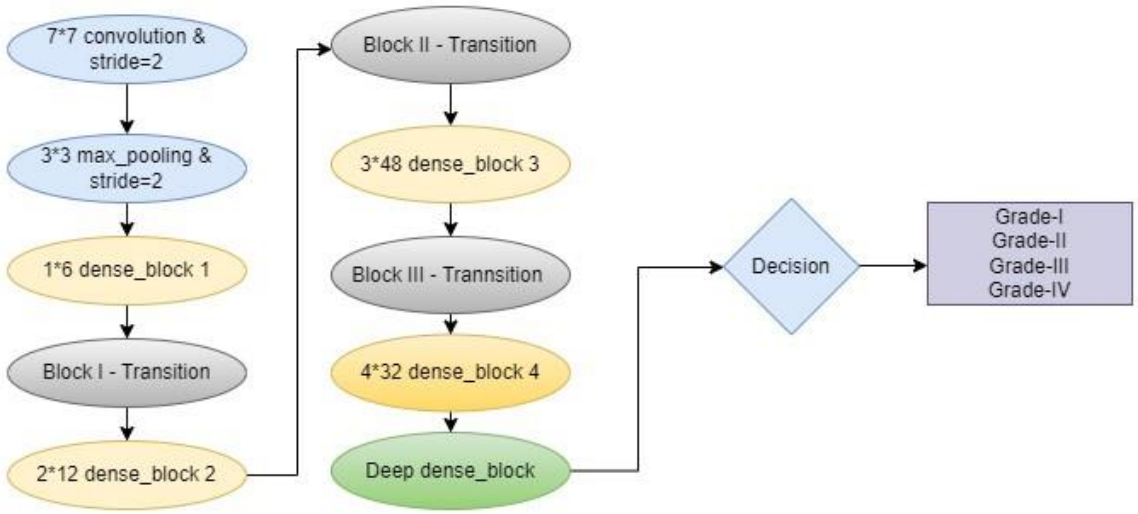

Fig. 8. Fine-tune DenseNet-169 architecture

The output layer generates a probability for each astrocytoma grades.

3.3.4 The proposed fine-tuned DenseNet-169

A CNN architecture called DenseNet-169 was developed to help deep networks address issues such as gradient vanishing and feature reuse. To address computational complexity, it employs bottleneck layers that use 1x1 convolutions to decrease the quantity of feature maps that are input. A brain MRI image is fed into the DenseNet-169 architecture, which highlights features indicative of the presence and severity of an astrocytoma. The network begins with a convolutional layer that reduces spatial dimensions by extracting fundamental characteristics. Feature maps are further down sampled by a max pooling layer, reducing computational complexity. There are four little blocks in the structure: 1x6 dense blocks I, 2x12 dense blocks II, 2x12 dense blocks III, 3x48 dense bricks and four 4x32 dense blocks IV, as illustrated in Fig. 8.

Each block has multiple layers, allowing for the efficient flow of information and gradients. A transition layer is applied to the network to minimize the number of characteristics while preserving the most essential ones. To capture ever more sophisticated and abstract properties, the network concatenates the outputs of each block with the inputs from later layers. To ensure that all relevant information is recorded before the final decision-making process, the final deep dense block integrates characteristics learnt from earlier layers. In this study, DenseNet169 has been fine-tuned to adapt to brain tumor grading by leveraging initial feature weights and optimizing them via backpropagation.

Initial Feature Weights

Pre-trained weights derived from comprehensive datasets (ImageNet) are used to initialize the layers of the refined DenseNet-169. These pre-trained weights offer a robust foundation, capturing low- and mid-level characteristics crucial to fundamental image processing, including edges, textures, and patterns. The fine-tuning method for astrocytoma grading gradually adapts these initial feature weights to the specific characteristics of MRI images of astrocytoma, including size, morphology, and contrast variations in T1-weighted, T2-weighted, and FLAIR sequences. To improve classification accuracy, DenseNet-152 may be fine-tuned to retain its powerful pre-trained characteristics while focusing on acquiring do-main-specific information crucial for discriminating against astrocytoma grades. The modification to these weights is given by Eq. (6):

Table 2. Results as per the evaluation measures for ResNet-152, VGG-19, MobileNetV3, and Fine-tuned DenseNet- 169

Experimental model utilized in this research	Grading system for astrocytoma tumors	Specificity	Sensitivity	Precision	Recall	F1score	Overall Accuracy
ResNet-152	Grade-I	0.96	0.97	0.98	0.97	0.96	96.34%
	Grade-II	0.95	0.96	0.96	0.96	0.95	
	Grade-III	0.96	0.97	0.95	0.98	0.97	
	Grade-IV	0.96	0.98	0.97	0.95	0.98	
VGG-19	Grade-I	0.97	0.98	0.98	0.96	0.98	95.22%
	Grade-II	0.95	0.96	0.96	0.95	0.95	
	Grade-III	0.98	0.97	0.97	0.98	0.96	
	Grade-IV	0.96	0.96	0.95	0.97	0.98	
MobileNetV3	Grade-I	0.96	0.98	0.96	0.96	0.97	97.42%
	Grade-II	0.97	0.97	0.98	0.95	0.96	
	Grade-III	0.97	0.96	0.96	0.97	0.95	
	Grade-IV	0.98	0.97	0.97	0.98	0.98	
Fine-tune DenseNet-169	Grade-I	0.99	0.99	0.99	0.99	0.99	99.68%
	Grade-II	0.99	0.98	0.99	0.99	0.99	
	Grade-III	0.99	0.99	0.99	0.99	0.99	
	Grade-IV	0.99	0.99	0.99	0.99	0.90	

$$W_n = W_{pre-train} - \eta . \frac{\partial £}{\partial W_{pre-train}} . \quad (6)$$

Weight Optimization

The application of weight optimization techniques yields accurate astrocytoma grade categorization with a fine-tuned DenseNet-152. It is first trained on a pre-trained set of weights from the large ImageNet dataset and then modified for astrocytoma grading using gradient descent and backpropagation. Weight optimization efficiently minimizes a function known as the loss, typically taken to represent categorical cross-entropy, to enhance a model's performance.

This is because the Adam optimizer is better for fi-ne-tuning, as it has momentum to reduce fluctuations and enhance convergence, as well as a time-varying learning rate. The adjusted weights are calculated with Eq. (7):

$$W_{\_n} = W_o - \eta . \Delta £(W) . \quad (7)$$

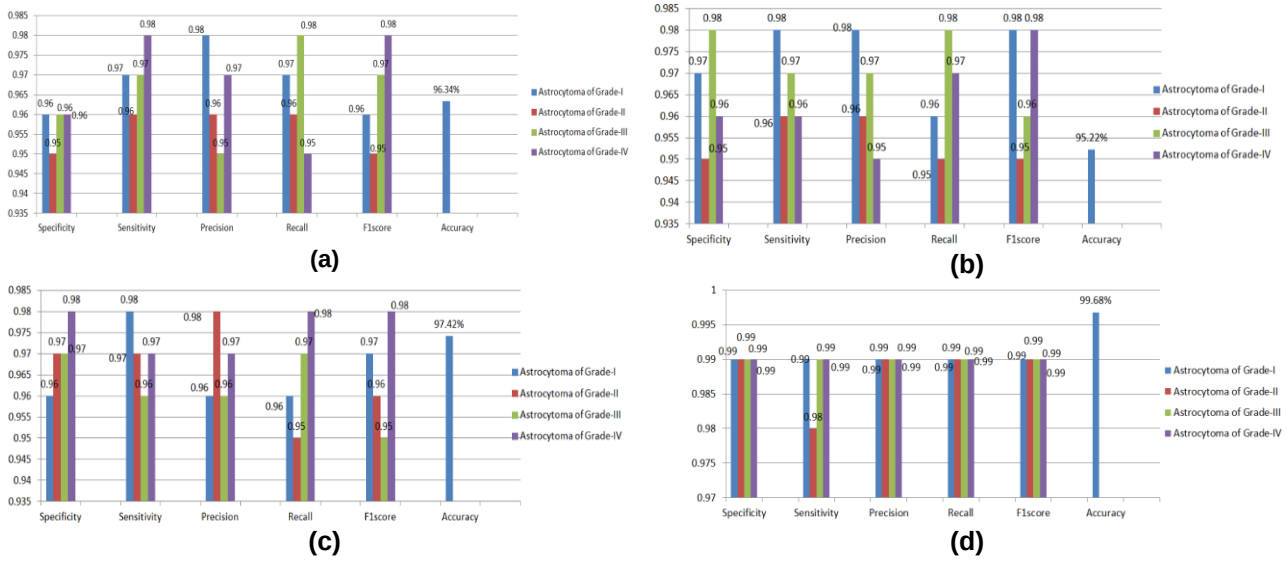

Fig. 9. Performance comparison of the four astrocytoma grades based on specificity, sensitivity, precision, recall, F1-score, and accuracy, presented as bar graphs: Grade I, II, III, and IV: (a) evaluation metrics obtained via ResNet-152; (b) evaluation metrics obtained via VGG-19; (c) evaluation metrics obtained via MobileNetV3; and (d) evaluation metrics obtained via Fine-tuned Dense-Net-169.

3.4 Experimental Setup

Multiple performance measures were used to assess the suggested astrocytoma grading categorization scheme. The Anaconda 2.6.0 environment was used to implement the model using Python utilizing TensorFlow and Keras (version 2.6.0). TensorFlow 2.6.0 was used as the backend within a system equipped with Python 3.9.18, an Intel Core i9-13950HX CPU (2.20GHz), 64GB RAM, and an 8GB Nvidia GeForce RTX 4060 GPU.

Figure 10 illustrates the accuracy and loss curves for both training and validation phases across the transfer learning models ResNet-152, VGG-19, MobileNetV3, and fine-tuned DenseNet-169. For multiclass classification, ROC diagrams illustrating the area beneath the curve (AUC) generated with a one-vs-rest approach showed average AUCs of about 0.99 across all grades. These numbers show that the model has good discrimination, particularly when it comes to identifying cases of advanced-grade astrocytoma. The confidence intervals suggest a narrow margin of variation.

4 Results and Discussion

This section presents the results of the experimental evaluation of astrocytoma grading using brain MRI images, accompanied by relevant explanations.

4.1 Results Obtained through ResNet-152, VGG-19, MobileNetV3 and Fine-tuned DenseNet-169

For the non-invasive evaluation of cerebral MRI images of astrocytoma's. The Res-Net-152 model performed well across all four, as seen in Table 1. Grade I, exhibiting F1-scores of 0.96, 0.97 specificity, 0.98 sensitivity, 0.97 accuracy, and 0.96 for recall. The results for Grade-II astrocytoma are noteworthy, with an F1-score of 0.95, sensitivity of 0.96, accuracy of 0.96, recall of 0.96, and specificity of 0.95. This grade demonstrates how well the model can accurately and consistently diagnose Grade-II astrocytoma. The model achieved an F1-score of 0.97, 0.96 specificity, 0.97 sensitivity, 0.95 precision, 0.98

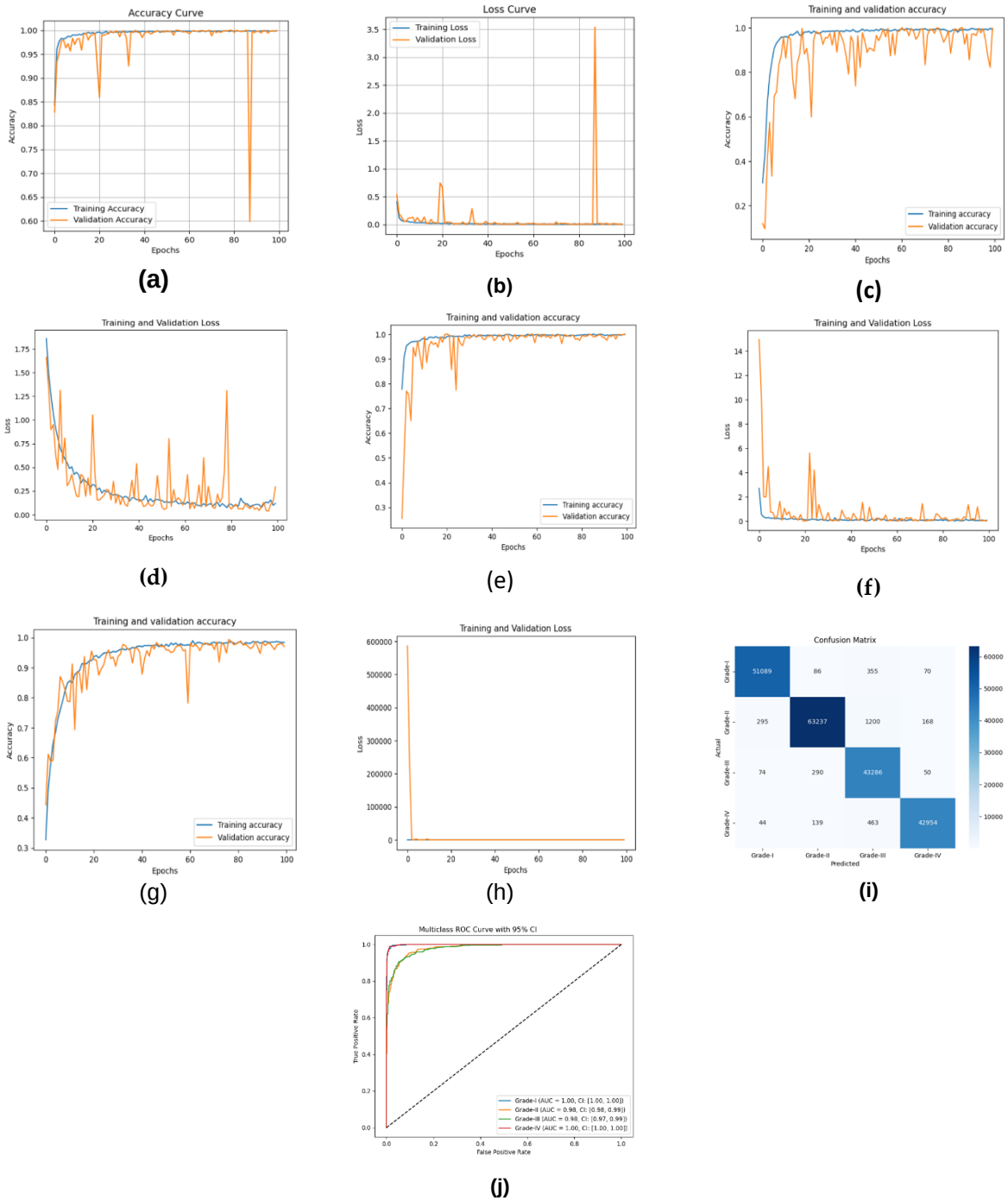

Fig. 10. Performance metrics for training and validation of the transfer learning models Res-Net-152, VGG-19, MobileNetV3, and fine-tuned DenseNet-169. Panels (a) and (b) depict the training and validation accuracy and loss of ResNet-152; (c) and (d) illustrate the corresponding accuracy and loss curves for VGG-19; (e) and (f) present the training and validation accuracy and loss of MobileNetV3; and (g) and (h) exhibit the same performance metrics for fine-tuned DenseNet-169. Panel (i) displays the confusion matrix for the fine-tuned DenseNet-169, whereas panel (j) illustrates the one-vs-rest ROC curve for multiclass classification, accompanied by the 95% confidence interval of the AUC values

recall, and high accuracy in distinguishing Grade-III astrocytoma's. Thus, when compared to other grades, the model does a good job of categorizing these tumors.

For the most aggressive variant (Grade-IV astrocytoma), the model's specificity was 0.96 and sensitivity were 0.98, while it's precision 0.97 and recall were 0.95. This resulted in an overall accuracy of 96.34%, as shown in Fig. 9(a). The results of this research show that the model is effective in identifying high-grade astrocytoma's, which is important for treatment and recovery procedures.

The study's findings, utilizing the VGG-19 model, concentrated on transfer learning for the non-invasive assessment of brain MRI astrocytoma's. The model performs effectively across all astrocytoma grades examined. The results for Grade-I astrocytoma are as follows: specificity, sensitivity, accuracy, recall, and F1-score are 0.97, 0.98, 0.98, 0.96, and 0.98, respectively. The model's Grade-II astrocytoma results are likewise favorable, with recall, specificity, sensitivity, accuracy, and F1-score all at 0.95. Even with Grade-III astrocytoma's, the model continues to perform well, with specificity 0.98, sensitivity 0.97, precision-recall 0.97, and F1-scores 0.96; it categorizes Grade-III tumors without sacrificing recall or precision. For the most severe scenario, astrocytoma Grade-IV, the VGG-19 model performs well, achieving 0.96 specificity, 0.96 sensitivity, 0.95 accuracy, 0.97 recall, and 0.98 F-1 score. 95.22% classification accuracy supports its excellent accuracy and precision in identifying and classifying the aggressive astrocytoma subtype, as shown in Fig. 9(b).

The MobileNetV3 approach achieved a respectable level of accuracy in classifying all astrocytoma grades in tests for the non-invasive evaluation of astrocytoma, utilizing brain MRI images. The model's performance for Grade-II astrocytoma's was 0.97 in specificity, 0.97 in sensitivity, 0.98 in accuracy, 0.95 in recall, and 0.96 in F1-score. In contrast, Grade I astrocytoma's had higher specificity, sensitivity, precision, recall, and F1-score of 0.96, 0.98, 0.96, 0.96, and 0.97, respectively.

During the grade-wise evaluation, MobileNetV3 exhibited specificity, sensitivity, accuracy, recall, and an F1-score of 0.97, 0.96, 0.96, 0.97, and 0.95, respectively, indicating that it is also appropriate for Grade III astrocytoma's. Furthermore, for Grade-IV Astrocytoma, the MobileNetV3 model's performance was above expectations, with specificity, sensitivity, accuracy, recall, and F1-score reported at 0.98, 0.97, 0.97, 0.98, and 0.98, respectively. MobileNetv3 achieved 97.42% overall accuracy, as shown in Fig. 9(c).

Across all astrocytoma grades, the Fine-tuned DenseNet-169 model demonstrated remarkable performance for non-invasive astrocytoma grading from brain MRI scans. For Grade I astrocytoma's, Table 1 shows specificity, sensitivity, accuracy, recall, and an F1-score of 0.99, 0.99, 0.99, 0.99, 0.99, respectively. These metrics demonstrate that the Fine-tuned DenseNet-169 model can reliably classify Grade-I astrocytoma with a low FP and FN rates. The model exhibits commendable performance, achieving specificity, sensitivity, accuracy, recall, and an F1-score of 0.99, 0.98, 0.99, 0.99, and 0.99 for Grade II astrocytoma.

The fine-tuned Dense-Net-169 model continues to show remarkable performance in the instance of Grade III astrocytoma, achieving 0.99 for F1-score, 0.99 for specificity, 0.99 for sensitivity, 0.99 for accuracy, and 0.99 for recall. The model maintains a good balance between sensitivity and specificity, minimizes misclassification rates, and accurately identifies Grade-III cancers. The Fine-tuned Dense-Net-169 model has exceptional performance for Grade IV astrocytoma, achieving specificity, sensitivity, F1-score, recall, and accuracy of 0.99, the most aggressive kind of astrocytoma. According to Fig. 9(d), the Fine-tuned DenseNet-169 model achieves an overall classification accuracy of 0.9968, indicating it can identify and classify the most severe astrocytoma, enabling efficient diagnosis and treatment planning. The application of ResNet-152, VGG-19, MobileNetV3, and Fine-Tuned DenseNet-169 architectures improved astrocytoma tumor grading accuracy. The model was trained to distinguish astrocytoma grades using preprocessed MRI images. The model's ability to reduce error rates and achieve peak performance in distinguishing between astrocytoma grades

Table 3. Comparison of the results with the state-of-the-art methods

Related work	Method	Dataset	Evaluation measures
[34]	SVM, fast large margin classifier, random forest classifier	The Cancer Genome Atlas (TCGA)	Sensitivity: 96.40% Specificity: 97.10% Accuracy: 95.80%
		The customize dataset	Accuracy: 91.00%
[35]	CNN	BraTS	Accuracy: 96.69%
		The customize dataset	Accuracy: 96.20%
[36]	Hybrid YOLOv5 and ResNet50	TCGA	Accuracy: 97.20% Precision: 98.60% Sensitivity: 98.60%
		The customize dataset	Accuracy: 95.20% Precision: 96.40% Sensitivity: 95.34%
[37]	CNN	Brain tumor MRI	Accuracy: 95.00%
Transfer learning models	ResNet-152	The customize dataset	Accuracy: 96.34%
	VGG-19		Accuracy: 95.22%
	MobileNetv3		Accuracy: 97.42%
The proposed	Fine-tuned DenseNet-169		Accuracy: 99.68%

was demonstrated by the continuous reduction in both training and validation losses.

4.2 Comparison of the Results

Table 2 compares the proposed approach with several leading state-of-the-art methods. This work is contrasted with previous significant advancements in this field, which employed a variety of methods and ML techniques to identify and classify brain tumors. Every study focuses on a distinct set of methods and evaluation criteria to improve the robustness and precision of cerebral MRI data categorization. [27] The Cancer Genome Atlas (TCGA) dataset was examined using two classifiers: support vector machine (SVM) and random forest, achieving commendable assessment metrics: producing sensitivity, specificity, and overall accuracy metrics of 96.4%, 97.1%, and 95.8%, respectively. [28] Developed a convolutional neural network with the BraTS dataset, attaining an accuracy of 96.69%. [29] A hybrid framework integrating YOLOv5 and ResNet50 was utilized on the TCGA dataset, achieving an accuracy of 97.2%, with precision and sensitivity both attaining 98.6%.

Furthermore, transfer learning architectures such as ResNet-152, VGG-19, and MobileNetV3 were utilized on an adapted dataset created for astrocytoma grading. The models attained accuracy rates of 96.34%, 95.22%, and 97.42%, respectively. This study assessed previously established state-of-the-art procedures on a bespoke dataset created for astrocytoma grading. The method described in [34] yielded an overall accuracy of 91% when applied to the customized dataset, which was considered inadequate. Similarly, the implementation of the method proposed by [28] utilizing the tailored dataset resulted in a significant accuracy of 96.2%. Conversely, the method described in [29] achieved an accuracy of 95.2%, precision of 96.4%, and sensitivity of 95.34% when evaluated on the customized dataset. [30] Implemented a CNN-based approach using Brain tumor MRI images with 95% accuracy. The results obtained with the Fine-tuned Dense-Net-169 showed

superior performance, with better accuracy across all grades compared to other studies.

It achieved an impressive 99.68% accuracy, highlighting the effectiveness of the fine-tuning approach in refining the model for specific classification tasks. Although DenseNet-169 is a deep architecture, it is designed with dense connectivity. This facilitates efficient feature reuse and reduces the total number of trainable parameters relative to other deep networks. For instance, DenseNet-169 comprises roughly 14 million parameters, significantly lower than VGG-19, which has around 143 million, while ResNet-152 comprises around 60 million. Thus, Dense-Net-169 offers improved memory efficiency and faster convergence during model training. Despite Mo-bileNetV3's remarkable efficiency and speed attributed to its lightweight architecture, its classification performance in our evaluation was inferior to that of DenseNet-169. Consequently, the proposed fi-ne-tuned DenseNet-169 model offers an advantageous balance between computational efficiency and predictive performance.

4.3 Limitations

While being extremely precise, the transfer learning architectures comprising ResNet-152, VGG-19, MobileNetV3, and DenseNet-169 might not be sufficient to account for patient-to-patient variation in other tumor traits. When new data is provided, such models may struggle to generalize, since they were trained to identify a predefined pattern in the training set. Transfer learning also implies the use of pre-existing models, which might not be the most appropriate for the unique characteristics of brain tumor MRI images. The information was gathered from a single hospital; thus, there may be institutional bias that limits the broad applicability of our methodology. The DenseNet-169 model, although demonstrating outstanding accuracy, poses challenges for clinical integration. Guaranteeing data protection and regulatory compliance is crucial. Real-time performance must be improved for application in healthcare settings. Moreover, discrepancies in MRI scanners and imaging methods may influence generalizability.

5 Conclusion and Future Work

This study examines the non-invasive categorization of astrocytoma's via brain MRI data with trans-former-based learning models. The MRI dataset utilized was sourced from Bahawal Victoria Hospital in Pakistan and comprised 230 patients diagnosed with Grades I, II, III, and IV astrocytoma's. This work utilized transfer learning models, namely Res-Net-152, VGG-19, MobileNetV3, and fine-tuned Dense-Net-169, to achieve accurate grading. The models exhibited the following accuracies: ResNet-50 at 96.34%, VGG-19 at 95.22%, MobileNetV3 at 97.42%, and fine-tuned DenseNet-169 at 99.68%. These models demonstrate how transfer learning can improve diagnostic accuracy by providing a strong foundation for non-invasive astrocytoma grading. The study highlights the practical implications of the pro-posed method, which may help radiologists with early diagnosis, reduce reliance on invasive procedures such as biopsies, and support individualized treatment planning, in addition to improving model performance. Future endeavors will encompass the integration of supplementary datasets, the use of sophisticated deep learning methodologies such as Graph Neural Networks, real-time deployment in clinical environments, and the investigation of multimodal strategies that amalgamate MRI data with alternative diagnostic modalities. It will also entail verifying the model across other institutions to enhance robustness. Furthermore, scanner variability was not explicitly accounted for, which may affect model performance across different MRI acquisition environments.

- Funding statement: No specific funding was received for this research.
- Conflict of interest: The authors declare no conflict of interest.
- Data availability: The datasets generated during the current study are available from the corresponding author upon request.

References

1. Venkatesan, D., Elangovan, A., Winster, H., Pasha, M. Y., Abraham, K. S.,

Niraikulam, A., Vellingiri, B. (2022). Diagnostic and therapeutic approach of artificial intelligence in neuro-oncological diseases. Biosensors and Bioelectronics: X, Vol. 11, 100188.

2. **Gilanie, G., Bajwa, U. I., Waraich, M. M., & Anwar, M. W. (2021).** Risk-free WHO grading of astrocytoma using convolutional neural networks from MRI images. Multimedia Tools and Applications, Vol. 80, No. 3, pp. 4295–4306.
3. **Yan, J. L., Li, C., van der Hoorn, A., Boonzaier, N. R., Matys, T., Price, S. J. (2020).** A neural network approach to identify the peritumoral invasive areas in glioblastoma patients by using MR radiomics. Scientific reports, Vol. 10, No. 1, pp. 9748.
4. **Ithayan, J. V., Sujitha, M. R., Karthikeyan, S., Jabakumar, A. K., Pavithra, M. L., Prabhavathy, M. S. (2023).** Machine learning approach for brain tumor detection. J. Surv. Fisheries Sci, Vol. 10, pp. 793–802.
5. **Nahar Metu, C. L., Sutihar, S. K., Sohel, M., Zohora, F., Hasan, A., Miah, M. T., Rahman, M. H. (2023).** Unraveling the signaling mechanism behind astrocytoma and possible therapeutics strategies: A comprehensive review. Cancer Reports, Vol. 6, No. 10, e1889.
6. **Aktipis, A. (2020).** The cheating cell: How evolution helps us understand and treat cancer.
7. **Nandi, P., Roy, S. (2022).** Tumor biology: An introduction. In Cancer Diagnostics and Therapeutics: Current Trends, Challenges, and Future Perspectives, Singapore: Springer Singapore pp. 43–55.
8. **Eibl, R. H., Schneemann, M. (2021).** Liquid biopsy and primary brain tumors. Cancers, Vol. 13, No. 21, 5429.
9. **Sareen, H., Garrett, C., Lynch, D., Powter, B., Brungs, D., Cooper, A., ... & Becker, T. M. (2020).** The role of liquid biopsies in detecting molecular tumor biomarkers in brain cancer patients. Cancers, Vol. 12, No. 7, 1831.
10. **Thakkar, J. P., Prabhu, V. C., Rouse, S., Lukas, R. V. (2020).** Acute neurological complications of brain tumors and immune therapies, a guideline for the Neuro-hospitalist. Current Neurology and Neuroscience Reports, Vol. 20, No. 8, pp. 32.
11. **Noureldine, M. H. A., Shimony, N., Jallo, G. I. (2023).** Benign spinal tumors. In Human Brain and Spinal Cord Tumors: From Bench to Bedside. Volume 2: The Path to Bedside Management Cham: Springer International Publishing, pp. 583–606.
12. **Mo, F., Pellerino, A., Soffietti, R., Rudà, R. (2021).** Blood–brain barrier in brain tumors: biology and clinical relevance. International journal of molecular sciences, Vol. 22, No. 23, pp. 12654.
13. **Kidd, D. P. (2023).** Neurological involvement by Behçet's syndrome: clinical features, diagnosis, treatment and outcome. Practical Neurology, Vol. 23, No. 5, pp. 386–400.
14. **Fu, Y., Jung, A. W., Torne, R. V., Gonzalez, S., Vöhringer, H., Shmatko, A., Gerstung, M. (2020).** Pan-cancer computational histopathology reveals mutations, tumor composition and prognosis. Nature cancer, Vol. 1, No. 8, pp. 800–810.
15. **Boutry, J., Tissot, S., Ujvari, B., Capp, J. P., Giraudeau, M., Nedelcu, A. M., Thomas, F. (2022).** The evolution and ecology of benign tumors. Biochimica et Biophysica Acta (BBA)-Reviews on Cancer, Vol. 1877, No. 1, 188643.
16. **Cano-Valdez, A. M., Sevilla-Lizcano, D. B. (2020).** Pathological classification of brain tumors. Principles of Neuro-Oncology: Brain & Skull Base, pp. 75–105.
17. **Gilanie, G., Bajwa, U. I., Waraich, M. M., Habib, Z., Ullah, H., Nasir, M. (2018).** Classification of normal and abnormal brain MRI slices using Gabor texture and support vector machines. Signal, Image and Video Processing, Vol. 12, No. 3, pp. 479–487.
18. **Steeg, P. S. (2021).** The blood–tumour barrier in cancer biology and therapy. Nature reviews Clinical oncology, Vol. 18, No. 11, pp. 696–714.
19. **Das, K. C., Rajagopalan, V., Rath, G. P. (2022).** Critical Care Management in Patients Undergoing Brain Tumor Surgery.

Oncocritical Care: An Evidence-based Approach, Singapore: Springer Nature Singapore, pp. 399-422.

20. **Khan, A. H., Abbas, S., Khan, M. A., Farooq, U., Khan, W. A., Siddiqui, S. Y., Ahmad, A. (2022).** Intelligent model for brain tumor identification using deep learning. Applied Computational Intelligence and Soft Computing, Vol. 2022, No. 1, 8104054.
21. **Gilanie, G., Bajwa, U. I., Waraich, M. M., Habib, Z. (2019).** Computer aided diagnosis of brain abnormalities using texture analysis of MRI images. International Journal of Imaging Systems and Technology, Vol. 29, No. 3, pp. 260–271.
22. **Jean-Quartier, C., Jeanquartier, F., Holzinger, A. (2020).** Open data for differential network analysis in glioma. International journal of molecular sciences, Vol. 21, No. 2, pp. 547.
23. **Tehsin, S., Nasir, I. M., Damaševičius, R. (2025).** Gatransformer: A graph attention network-based transformer model to generate explainable attentions for brain tumor detection. Algorithms, Vol. 18, No. 2, pp. 89.
24. **Poornam, S., Angelina, J.J.R. (2024).** VITALT: a robust and efficient brain tumor detection system using vision transformer with attention and linear transformation. Neural Computing and Applications, Vol. 36, No. 12, pp. 6403–6419.
25. **Christoforidis, G. A. (2022).** Low-grade astrocytomas. In Handbook of Neuro-Oncology Neuroimaging, Academic Press, pp. 521–545.
26. **Ohgaki, H., Kleihues, P. (2013).** The definition of primary and secondary glioblastoma. Clinical cancer research, Vol. 19, No. 4, pp. 764–772.
27. **Ullah, M. S., Khan, M. A., Masood, A., Mzoughi, O., Saidani, O., Alturki, N. (2024).** Brain tumor classification from MRI scans: a framework of hybrid deep learning model with Bayesian optimization and quantum theory-based marine predator algorithm. Frontiers in Oncology, Vol. 14, 1335740.
28. **Usuzaki, T., Takahashi, K., Inamori, R., Morishita, Y., Takagi, H., Shizukuishi, T., ... & Takase, K. (2024).** Grading diffuse glioma based on 2021 WHO grade using self-attention-base deep learning architecture: variable Vision Transformer (vViT). Biomedical Signal Processing and Control, Vol. 91, 106001.
29. **Reddy, K. R., Rajesh, K. N., Dhuli, R., & Kumar, V. R. (2024).** BrainCDNet: a concatenated deep neural network for the detection of brain tumors from MRI images. Frontiers in Human Neuroscience, Vol. 18, 1405586.
30. **Divya, B., Nair, R. P., Prakashini, K., Menon, G., Litvak, P., Mandava, P., Vijayasenan, D. (2024).** A hybrid CNN-FC approach for automatic grading of brain tumors from non-invasive MRIs. In 2024 Seventh International Women in Data Science Conference at Prince Sultan University (WiDS PSU), pp. 99–104.
31. **Priyadarshini, P., Kanungo, P., Kar, T. (2024).** Multigrade brain tumor classification in MRI images using Fine tuned Efficientnet. e-Prime-Advances in Electrical Engineering, Electronics and Energy, Vol. 8, 100498.
32. **Harati Kabir, V., Mahdavifar Khayati, R., Fallahi, A. (2023).** Non-invasive grading of brain tumors using online support vector machine with dynamic fuzzy rule-based parameters optimization. Proceedings of the Institution of Mechanical Engineers, Part H: Journal of Engineering in Medicine, Vol. 237, No. 6, pp. 727–740.
33. **Ali, M. B., Gu, I. Y. H., Berger, M. S., Jakola, A. S. (2023).** A novel federated deep learning scheme for glioma and its subtype classification. Frontiers in Neuroscience, Vol. 17, 1181703.
34. **Elazab, N., Gab Allah, W., Elmogy, M. (2024).** Computer-aided diagnosis system for grading brain tumor using histopathology images based on color and texture features. BMC Medical Imaging, Vol. 24, No. 1, pp. 177.
35. **Berghout, T. (2024).** The neural frontier of future medical imaging: A review of deep

learning for brain tumor detection. Journal of imaging, Vol. 11, No. 1, pp. 2.

36. **Elazab, N., Gab-Allah, W. A., Elmogy, M. (2024).** A multi-class brain tumor grading system based on histopathological images using a hybrid YOLO and RESNET networks. Scientific reports, Vol. 14, No. 1, pp. 4584.
37. **Simo, A. M. D., Kouanou, A. T., Monthe, V., Nana, M. K., Lonla, B. M. (2024).** Introducing a deep learning method for brain tumor classification using MRI data towards better performance. Informatics in Medicine Unlocked, Vol. 44, 101423.
38. **Lefebvre, E. (2008).** Fast Unfolding of Communities in Large Networks. Journal of Statistical Mechanics: Theory and Experiment, Vol. 2008, No. 10, pp. P10008.
39. **Rosvall, M., Bergstrom, C.T. (2008).** Maps of Random Walks on Complex Networks Reveal Community Structure. Proceedings of the National Academy of Sciences, Vol. 105, No. 4, pp. 1118–1123.

Article received on 16/02/2026; accepted on 18/03/2026.
**Corresponding authors is Oswaldo Morales Matamoros.*